DLL3 REGULATES NOTCH SIGNALING IN SCLC

Jun W. Kim[1,2#], Julie H. Ko[1,2#], and Julien Sage[1,2*]

Departments of [1]Pediatrics, [2]Genetics, Stanford University, Stanford, CA, USA.

[#]Equal contributions

*Correspondence to: Julien Sage, Stanford University, 265 Campus Drive, SIM1 G2078, Stanford, CA 94305-5457. Phone: 650-724-9246; Fax: 650-736-0195; E-mail: julsage@stanford.edu

ABSTRACT

Tumor heterogeneity plays a critical role in tumor development and response to treatment. In small-cell lung cancer (SCLC), intratumoral heterogeneity is driven in part by the Notch signaling pathway, which reprograms neuroendocrine cancer cells to a less/non-neuroendocrine state. Here we investigated the atypical Notch ligand, DLL3 as a biomarker of the neuroendocrine state and a regulator of cell-cell interactions in SCLC. We first built a mathematical model to predict the impact of DLL3 expression on SCLC cell populations. We next tested this model using a single-chain variable fragment (scFv) to track DLL3 expression *in vivo* and a new mouse model with inducible expression of DLL3 in SCLC tumors. We found that high levels of DLL3 promote the expansion of a new SCLC cell population with lower expression levels of both neuroendocrine and non-neuroendocrine markers. This work may influence how DLL3-targeting therapies are used in SCLC patients.

INTRODUCTION

Intratumoral heterogeneity is a hallmark of cancer, including a variety of cancer and non-cancer cells forming a tumor. This heterogeneity may vary over time and environmental conditions, including following therapy, and it can arise from genetic or epigenetic mechanisms. Intratumoral heterogeneity plays an important role in tumor development, including shaping the natural response of cancer cells to the immune system or treatment in the clinic (reviewed in (Black and McGranahan, 2021; Dagogo-Jack and Shaw, 2018; Jamal-Hanjani et al., 2015; Tammela and Sage, 2020)).

Small-cell lung cancer (SCLC) is an aggressive subtype of lung cancer with fast growth rates and a striking metastatic ability. The median overall survival of SCLC patients has remained close to 8-10 months in the past 3 decades, with a 5-year survival at ~6%, and over 200,000 estimated deaths worldwide every year. Most tumors respond initially well to standard-of-care chemoradiation treatment, but resistance emerges rapidly in nearly all cases (reviewed in (Rudin et al., 2021)). The recent approval of T-cell immune checkpoint inhibitors has been beneficial to only a small fraction of SCLC patients (reviewed in (Barrows et al., 2022)). There is a critical need to develop biomarkers for SCLC development and more efficient therapeutic strategies.

SCLC tumors have been classified in different subtypes based on transcriptional programs driven by specific transcription factors, with the SCLC-A (expressing the ASCL1 transcription factor) and SCLC-N (expressing the NEUROD1 transcription factor) neuroendocrine subtypes being the most frequent (Baine et al., 2020; Gay et al., 2021; Rudin et al., 2019). Importantly, mounting evidence indicates that individual SCLC tumors are comprised of heterogeneous populations of cancer cells with different levels of neuroendocrine gene programs (Calbo et al., 2011; Lim et al., 2017; Williamson et al., 2016). For example, in SCLC-A tumors, activation of Notch signaling can reprogram neuroendocrine (NE) cancer cells towards less/non-neuroendocrine (non-NE) phenotypes, and the non-NE cells can support the survival of the NE cells, including when tumors are treated with chemotherapy (Lim et al., 2017). In this context, the mechanisms activating Notch signaling are not completely understood, but may depend on the YAP transcriptional regulator (Shue et al., 2022). As another example, in SCLC-N tumors, expression of c-MYC can activate Notch signaling, which also promotes the transition of these tumors to a less neuroendocrine phenotype (Ireland et al., 2020). These data and

data from human tumors indicate that both inter- and intra-tumoral heterogeneity are likely key contributors of the ability of SCLC tumors to become resistant to therapies (Gay et al., 2021; Stewart et al., 2020; Sutherland et al., 2022).

DLL3 (Delta-like ligand 3) is an atypical ligand for NOTCH receptors initially studied for its role in early pattern formation in mouse embryos (Bulman et al., 2000; Dunwoodie et al., 1997; Kusumi et al., 1998). Early work showed that DLL3 is an inhibitor of Notch signaling in a cell autonomous manner (Ladi et al., 2005), possibly in a cis-inhibition mechanism in the Golgi of cells (Chapman et al., 2011; Geffers et al., 2007). However, genetic studies of DLL3 O-fucosylation indicate that interactions with NOTCH may not be sufficient for the physiological function of DLL3, suggesting possible Notch-independent roles for DLL3 *in vivo* (Serth et al., 2015). The mouse *Dll3* gene is a direct target of ASCL1 (Nelson et al., 2009). Importantly, Saunders and colleagues showed that DLL3 is present at the surface of SCLC cells and that targeting DLL3-expressing SCLC cells using an antibody-drug conjugate (ADC) can eradicate SCLC in pre-clinical models (Saunders et al., 2015). Clinical trials using Rovalpituzumab tesirine (Rova-T), an ADC targeting DLL3, have been largely unsuccessful due to toxic side effects of this molecule (e.g., (Blackhall et al., 2021; Johnson et al., 2021; Malhotra et al., 2021)). However, other strategies are being develop to target DLL3 expressing cells (e.g., (Giffin et al., 2021; Hipp et al., 2020; Lakes et al., 2020; Tully et al., 2022)) and DLL3 remains a target of interest for the detection and the treatment of SCLC.

Here we sought to develop tools and models to further investigate the role of DLL3 as a biomarker of SCLC and as a regulator of Notch signaling in SCLC. We used mathematical modeling based on published data to predict the potential role that DLL3 expression may have on tumor heterogeneity. We further developed a new single-chain fragment variable (scFv) that can bind DLL3 in cells and *in vivo.* Finally, we used this scFv to test our mathematical models in a new genetically engineered mouse model with inducible expression of DLL3. Our data show variable levels of DLL3 expression in SCLC and indicate that DLL3 expression contributes to intratumoral heterogeneity.

RESULTS

Modeling the role of DLL3 in Notch-driven intratumoral heterogeneity in SCLC

DLL3 is often viewed as a cis-inhibitor of Notch signaling during development because of its localization in the Golgi (**Figure 1A**). To determine if DLL3 could suppress Notch activity in SCLC cells, we used cells derived from tumors in the *Rb*$^{fl/fl}$*;p53*$^{fl/fl}$*;Rbl2*$^{fl/fl}$*;Hes1*^{GFP} mouse model of SCLC (the *Rb*$^{fl/fl}$*;p53*$^{fl/fl}$*;Rbl2*$^{fl/fl}$ model is known as the triple knockout model, *TKO*, and is also known as the *RPR2* model) (Lim et al., 2017; Shue et al., 2022). In this model, SCLC cells express GFP when the *Hes1* promoter is active. Because *Hes1* is a target of Notch signaling, GFP expression can serve as a reporter of Notch activity. We isolated HES1^{GFP}-positive (HES1^{pos}) cells from *RPR2;Hes1*^{GFP} mutant tumors; these cells are less/non-neuroendocrine (Lim et al., 2017; Shue et al., 2022). Ectopic expression of FLAG-tagged DLL3 in these HES1^{pos} cells led to fewer GFP-positive cells, providing further evidence that DLL3 can suppress Notch signaling in *cis* in this SCLC context (**Figure 1B-D** and **Supplementary Figure S1A**).

In the Notch signaling pathway, activation of NOTCH receptors by their ligands, such as Delta-like proteins (DLLs), leads to NOTCH cleavage, releasing the intracellular domain of NOTCH (NICD). NICD induces transcription of the gene coding for HES1, which is an inhibitor of ASCL1, itself an activator of the expression of DLLs (Nelson et al., 2009; Ohsawa and Kageyama, 2008). This negative feedback leads to lateral inhibition and distinct cell fates among neighboring cells: low Notch/high DLL ('sender') cells and high Notch/low DLL ('receiver') cells (**Figure 1A**) (Collier et al., 1996). To gain a better understanding of the consequences of DLL3 expression on Notch signaling and intratumoral heterogeneity in SCLC, we built a simple mathematical model by incorporating DLL3 in the mutual inhibition model of lateral inhibition (Sprinzak et al., 2010) using the following reactions: 1) NOTCH receptors, denoted N, and DLL1 (as a representative of DLLs), denoted D, bind in *trans*, which leads to cleavage of NOTCH and release of the Notch intracellular domain (NICD), denoted S; 2) NICD increases expression of HES1, denoted H (Bray 2006); 3) HES1 inhibits expression of DLL1; 4) NOTCH receptors bind to DLL1 and DLL3, denoted D3, in *cis*, which inhibits NOTCH cleavage (Miller et al., 2009; Chapman et al., 2010; Ladi et al., 2005). We simulated this model using 1600 parameter sets across a two-dimensional parameter space spanning a wide range of the production rates of D (β_D) and D3 (β_{D3}) (**Figure 1E**, **Equations 1-4** in

Methods section, and **Table S1** for parameter values). To represent multicellular interactions, a two-dimensional hexagonal cell lattice was used for each parameter set. We plotted log(H_{max}/H_{min}), where H_{max} and H_{min} are the maximal and minimal HES1 levels in the hexagonal lattice at the steady state, as a function of β_D and β_{D3} to observe parameters leading to lateral inhibition, or heterogeneity in HES1 level (Formosa-Jordan and Sprinzak 2014).

The cis-inhibition model shows that when $\beta_{D3} > \beta_D$ HES1 heterogeneity mostly do not occur, indicating effective inhibition of cell-type bifurcation (**Figure 1E**). Within the heterogeneity parameter regime, β_{D3} also regulates the ratio of receiver (H^{high}) cells and sender (H^{low}) cells, with higher number of sender cells as β_{D3} increases (**Figure 1F**). We next examined H_{max} and H_{min} separately. H_{max} consistently decreases as β_{D3} increases (**Figure 1G**). Interestingly, a large region of parameter space show higher H_{min} with DLL3 (**Figure 1H,I**). H_{min} increases throughout the heterogeneity parameter regime, peaking near $\beta_{D3} = \beta_D$, and gradually decreases as β_{D3} further increases (**Figure 1H**).

In this system, the modeling suggests that while DLL3 can inhibit lateral inhibition, its effect on intratumoral heterogeneity driven by Notch signaling may depend on the levels of DLL3. At high levels ($\beta_{D3} >> \beta_D$), DLL3 inhibits both heterogeneity and Notch activation. But at lower levels DLL3 allows trans-interaction between NOTCH and other DLLs while preventing lateral inhibition, which leads to homogeneous intermediate NOTCH activation throughout the cell population. In the heterogeneity parameter region DLL3 expression also affected sparsity of the receiver cells.

Generation and validation of a single-chain fragment variable (scFv) binding DLL3

Determining DLL3 levels in SCLC cells may be important to determine if anti-DLL3 strategies should be used in individual patients with SCLC. Our mathematical modeling data further suggest that monitoring DLL3 levels in tumors *in vivo* may be important to gain a better understanding of intratumoral heterogeneity in SCLC tumors. We next sought to develop a new tool to detect DLL3 in tumors *in vivo.*

Single-chain fragment variables (scFvs) have several advantages over antibodies, including their small size and their ease of production in bacteria (Peltomaa et al., 2022; Weisser and Hall, 2009). We generated a His-tagged scFv based on the sequence of an antibody targeting DLL3 (Methods) (**Figure 2A and Supplementary Figure S2A**). We

first tested the binding of this scFv targeting DLL3 in 293T cells expressing exogenous DLL3 compared to controls. Flow cytometry analysis using an anti-His antibody showed increased binding in cells expressing mouse DLL3 (**Figure 2B,C**). Using the same approach, we were also able to detect endogenous DLL3 expression in human SCLC cell lines (**Figure 1C** and **Supplementary Figure S2B**). Thus, this scFv targeting DLL3 is capable of binding to DLL3 expressed on the surface of SCLC cells in culture.

To determine if this scFv molecule (aDLL3scFv) could be useful to detect SCLC tumors *in vivo*, we directly labeled it with Alexa Flour 680 (AF680), a near-infrared fluorophore with strong tissue penetration that is suitable for in vivo imaging, to the amino groups of lysine residues and the N-terminal group of the scFv (**Figure 1D**). We verified that the AF680 labeled anti-DLL3 scFv (aDLL3AF680) still detected DLL3 on the surface of SCLC lung cancer cells in culture (**Figure 1E,F** and **Supplementary Figure S2C**). Non-invasive optical imaging was performed over 6 h time period after we performed tail-vein injections with 2 nmol of aDLL3AF680 in NSG mice bearing subcutaneous xenografts (NCI-H82 model). Whole-body fluorescent imaging showed prominent signal in the tumor area, as well as in the kidney (where the scFv molecules are excreted) 2-3 hours post injection (**Figure 2G,H**). Maximum tumor-to-normal tissue contrast was observed 2 hours post injection (**Supplementary Figure S2D**). Signal from the fluorescent scFv was strong after 1 hour and started to decrease after 3-4 hours, as expected for a small molecule with a short half-life (**Figure 2I**).

Exogenous expression of DLL3 in mouse SCLC tumors

Notch signaling is a driver of non-neuroendocrine cell fates and intratumoral heterogeneity in SCLC (Ireland et al., 2020; Lim et al., 2017), and our mathematical modeling predicts that DLL3 may contribute to Notch signaling activity and may modulate heterogeneity. We next sought to test this idea experimentally in the *RPR2* mouse model of SCLC where this heterogeneity has been described (Lim et al., 2017; Shue et al., 2022). In this model, intra-tracheal instillation of an adenoviral vector expressing the Cre recombinase initiates tumors modeling the SCLC-A subtype of human SCLC. SCLC cells in these tumors express DLL3 at their surface (**Figure 3A** and **Supplementary Figure S3A**).

To manipulate DLL3 levels in this model, we generated a new allele to conditionally induce DLL3 expression upon Cre-mediated recombination (*Rosa26*$^{LSL\text{-}Dll3}$ allele) (**Figure**

3A). We crossed this allele to the *RPR2* model (*RPR2;Rosa26*$^{LSL\text{-}Dll3}$ mice) and initiated tumors by Ad-CMV-Cre instillation. As controls, we used *RPR2;Rosa26*$^{LSL\text{-}Luc}$ mice (Jahchan et al., 2016). Tumors developed in *RPR2;Rosa26*^{Dll3} mice, and their histology was indistinguishable from that of *RPR2;Rosa26*^{Luc} mice; while we did not generate enough mice to rigorously quantify tumor number and tumor burden, we did not observe any striking difference in tumor development between the two models (**Figure 3B**). A cell line derived from a *RPR2;Rosa26*^{Dll3} mutant lung tumor grew as spherical clusters in suspension typical of neuroendocrine SCLC cell lines (Lim et al., 2017) and showed weak but detectable expression of the tdTomato reporter linked to DLL3 expression, as well as the expected recombination of the *Lox-STOP-Lox* cassette, validating the new allele (**Figure 3A** and **Supplementary Figure S3B,C**).

We analyzed tumors from *RPR2;Rosa26*^{Dll3} and *RPR2;Rosa26*^{Luc} mutant mice ~5-6 months after tumor initiation for DLL3 expression using aDLL3scFv. In control *RPR2;Rosa26*^{Luc} tumors, we observed two populations of cancer cells, as would be expected for tumors with neuroendocrine (high DLL3) and less/non-neuroendocrine (low DLL3) cells (**Figure 3C,D**). We validated this using NCAM and ICAM staining, with NCAM^{high} ICAM^{low} cells representing neuroendocrine cells and NCAM^{low} ICAM^{high} cells representing less/non-neuroendocrine, as determined previously by RNA-sequencing of these two populations from *RPR2* tumors (Shue et al., 2022) (**Figure 3E,F**). In *RPR2;Rosa26*^{Dll3} mutant tumors, we observed fewer cells with low levels of DLL3 and a more homogeneous population of cells expressing intermediate/high levels of DLL3 (**Figure 3C,D**), indicating that the *Rosa26*^{DLL3} allele can elevate DLL3 expression on the surface of DLL3^{low} cells but does not result in further overexpression on the surface of DLL3^{high} cells (**Figure 3C,D**). Similarly, while NCAM^{high} ICAM^{low} cells express higher level of DLL3 compared to NCAM^{low} ICAM^{high}, no significant difference was detected between those of NCAM^{high} ICAM^{low} cells and cells from *RPR2;Rosa26*^{Dll3} mutant tumors (**Figure E, F**).

We next quantified HES1 expression as a marker of intratumoral heterogeneity in *RPR2;Rosa26*^{Dll3} and *RPR2;Rosa26*^{Luc} mutant tumors, HES1^{high} cells being Notch-active cells and less/non-neuroendocrine. As expected, we found regions with variable numbers of HES1-positive cells (Lim et al., 2017; Shue et al., 2022) (**Supplementary Figure S3D**). However, we did not detect any significant change in heterogeneity based on this marker

between the two groups (**Supplementary Figure S3E**). While these experiments indicate that higher levels of DLL3 in tumors do not block the ability of SCLC cells to undergo a transition to a Notch-driven HES1-positive state, we reasoned that immunostaining may not be quantitative enough to identify more subtle changes.

We expected that higher overall levels of DLL3 may alter the ratio between neuroendocrine and less/non-neuroendocrine cells by perturbing Notch signaling. Based on our data (**Figure 3C-F**), we also expected higher proportion of cells in *RPR2;Rosa26*^{Dll3} tumor to be NE (NCAM^{high} ICAM^{low}). However, cells from *RPR2;Rosa26*^{Dll3} tumors showed different distribution of NCAM^{high} ICAM^{low} cells and NCAM^{low} ICAM^{high} cells compared to that of *RPR2;Rosa26*^{Luc} mutant tumors (**Figure 3G-I**). Notably, *RPR2;Rosa26*^{Dll3} tumors exhibited a decrease in both NCAM^{high} ICAM^{low} and NCAM^{low} ICAM^{high} populations, which was also reflected by an increase in NCAM^{low} ICAM^{low} cells **(Figure 3J**). The relatively homogeneous population in *RPR2;Rosa26*^{Dll3} tumors suggests that higher expression of DLL3 in SCLC cells can inhibit the cell-fate bifurcation process mediated by Notch signaling pathway. Our mathematical modeling leads to the prediction that inhibition of lateral inhibition by DLL3 can prevent the rise of both sender and receiver cells as shown in the parameter regime where $\beta_{D3} > \beta_D$ with relatively higher HES1 levels. These observations support a model in which DLL3 contributes to Notch signaling activity in SCLC and may serve as a Notch pathway inhibitor in SCLC tumors *in vivo*.

Discussion

Here we investigated the role of the atypical NOTCH ligand DLL3 in a mouse model of SCLC. In our three-prong approach, we combined mathematical modeling, a new scFv molecule, and a new allele to induce DLL3 expression in mouse cells. We found that DLL3 expression contributes to the generation of specific subpopulations of SCLC cells, supporting a role for DLL3 in Notch signaling and in the control of intratumoral heterogeneity in SCLC.

While cell autonomous sources for intratumoral heterogeneity arise from various stressors and defects that generate genetic instability, non-cell autonomous contributors often involve signaling pathways that play critical roles during normal development and that can modify the transcriptome of cancer cells. In this regard, a canonical process involves spatiotemporal regulation of the Notch signaling pathway. The Notch pathway is an evolutionarily highly conserved signaling mechanism that is also implicated in the development and the progression of various cancer types. In different tissues, Notch signaling provides a binary fate switch through biochemical feedback mechanism known as lateral inhibition, which regulates differentiation into different cancer cell types from an initially homogenous field of cells (reviewed in (Chitnis, 1995; Sjöqvist and Andersson, 2019)). Thus, in the context of lateral inhibition Notch signaling pathway promotes cell fate “bifurcation”, rather than a specific cell fate. This contribution of Notch-mediated lateral inhibition to intratumoral heterogeneity has been investigated extensively in multiple settings, including breast cancer (Bocci et al., 2019), glioblastoma (Lim et al., 2015), or bladder cancer (Torab et al., 2021). To examine a potential role of DLL3 in SCLC in the classical Notch circuit, we incorporated DLL3 in the lateral inhibition with mutual inactivation model. Our mathematical modeling predicts that DLL3 expression can affect Notch signaling in several ways. As expected, when the production rate of DLL3 exceeds that of DLL1 ($\beta_{D3} > \beta_D$) heterogeneity sharply decreases indicating that DLL3 effectively reduces lateral inhibition. Within the parameter regime of heterogeneity (**Figure 1E**), DLL3 expression modulates the relative number of HES1^{pos} cells and making them sparser with increased DLL3 expression (**Figure 1F**). Interestingly, while very high production rates of DLL3 ($\beta_{D3} >> \beta_D$) lead to inhibition of Notch activation in the entire population, over a wide range of parameters DLL3 expression maintained intermediate level of Notch activation, which peaks near $\beta_{D3} = \beta_D$ (**Figure 1H,I**). This observation

reflects two seemingly opposing effects on Notch signaling. Low levels of DLL3 are sufficient to inhibit lateral inhibition, reducing or preventing the rise of HES1^{low} cells. At very high levels, DLL3 inhibits Notch activation entirely through complete cis-inhibition. In between these two states, the trans-activation of Notch by DLL1 reinforces intermediate Notch activity even within the homogeneity parameter regime. Thus, in the context of SCLC, our theoretical framework predicts that while high levels of DLL3 promotes HES1^{low} phenotype (neuroendocrine), at lower levels it can lead to a hybrid phenotype that is neither HES1^{low} nor HES1^{high}. When we examined the role of DLL3 experimentally in these processes, we found that ectopic expression of DLL3 in HES1^{pos} cells results in decreased HES1 expression, supportive of a cis-inhibitory function for DLL3. Intriguingly, induction of DLL3 in a mouse model of SCLC revealed that this ectopic expression decreases the relative number of both the neuroendocrine (NCAM^{high} ICAM^{low}) and non-neuroendocrine (NCAM^{low} ICAM^{high}) populations of cancer cells. This result suggests that DLL3 inhibits the bifurcation of SCLC cell fates. It will be interesting to examine in future studies the exact nature of the NCAM^{low} ICAM^{low} population in *RPR2;Rosa26^{Dll3}* tumors, for example whether these cells represent a precursor cell similar to lung epithelial cells early during lung development before Notch signaling is activated. Our new mouse allele for DLL3 expression may also be useful to investigate how DLL3 plays Notch-dependent and Notch-independent roles both in developmental processes and in cancer.

Because several therapeutic approaches currently in clinical development rely on the expression of DLL3 on SCLC cells validating its expression before and during the treatment could benefit patients with SCLC. Monitoring DLL3 levels in SCLC cells could be used to track overall progression of SCLC and, as our data suggest, heterogeneity between SCLC cell subpopulations. PET imaging of DLL3 have been evaluated clinically using DLL3 targeting antibodies with promising results (Sharma et al., 2017). However, the slow normal tissue clearance and requirement of radioisotopes with long half-lives hamper clinical application of antibodies as noninvasive imaging agents (Wei et al., 2020). Here, we generated an anti-DLL3 scFv (~1/8th the size of an antibody) labeled with a fluorophore (aDLL3AF680) with tissue penetration, allowing noninvasive optical imaging. aDLL3AF680 successfully labeled SCLC tumors *in vivo* with good tumor-to-normal tissue contrast in a short time frame (2 hours post injection). Fast clearance may lead to a superior imaging agent for clinical application. Small size may allow better tissue penetration. Thus, scFv may be a great alternative to full-length antibody for *in vivo*

detection and targeting of DLL3 in SCLC and other tumor types expressing this molecule on their surface.

Methods

Ethics statement

Mice were maintained according to practices prescribed by the National Institute of Health at Stanford's Research Animal Facility (protocol 13565) and by the Institutional Animal Care and Use Committee (IACUC) at Stanford. Additional accreditation of Stanford animal research facility was provided by the Association for Assessment and Accreditation of Laboratory Animal Care.

Synthesis of anti-DLL3 scFv

Escherichia coli BL21 (DE3) cells were transformed with anti-DLL3 scFv (Raum et al., 2017) with c-terminal hexahistidine tag in pET vector by VectorBuilder. The transformed cells were grown overnight in LB agar plates with 100 μg/mL ampicillin. Single colony from each plate was inoculated in LB broth containing ampicillin and grown overnight. The primary culture was diluted 1:100 and grown at 37ºC. When OD_{600} reached 0.5 the cells were induced with IPTG 0.5 mM at 37ºC for 6 h. The cells were then harvested by centrifugation at 3,500 g and the cell pellet was re-suspended with B-PER reagent (Thermo Fisher Scientific 90084) with lysozyme (0.1 mg/mL) and DNase I (50 µg/mL) and incubated for 30 min at 37ºC. Lysates were centrifuged at 15,000 × *g* for 10 min and the supernatants were purified using a nickel-NTA affinity column (Qiagen 30210). Centrifugal filters with molecular 10 kDa molecular weight cutoffs (Millipore UFC801024) were used for further purification and buffer exchange into PBS. Protein purity was further analyzed using sodium dodecyl sulfate polyacrylamide gel electrophoresis and quantified using a plate reader.

AF680 dye conjugation

Purified scFv was buffer-exchanged to 0.1 M sodium bicarbonate buffer (pH 8.3) and concentrated to 3 mg/mL. AF680 succinimidyl ester (Thermo Fisher Scientific A20008) was dissolved in DMSO at 10 mg/mL and added to the protein solution to give a final concentration of 1 mg/mL. The reaction was incubated for 1 hr at room temperature. Unreacted dye was removal and buffer exchange to PBS was done using a 10 kDa centrifugal filter.

Cell Binding assays

$5x10^5$ human and mouse cell lines were incubated with 50 µL of 30 µg/mL aDLL3AF680 for 1 hr in PBS with 0.1% BSA (PBSB) at 4ºC. The cells were then washed twice with PBSB and analyzed by flow cytometry using. For testing unlabeled aDll3scFv, cells were incubated with 50 µL of 30 µg/mL aDll3scFv for 1 hr in PBSB at 4ºC. The cells were washed once with PBSB and secondary binding was performed on ice for 30 min using rabbit anti-hexahistidine antibody (Cell Signaling Technology 12698S) diluted 1:100 in PBSB. The cells were washed once with PBSB and incubated with goat anti-rabbit antibody labeled with Alexa Fluor 488 (Invitrogen A11008) diluted 1:100 in PBSB for 30 min on ice. The cells were then washed twice with PBSB before analyzed by flow cytometry.

Cell culture

Cell lines were cultured in RPMI-1640 (Corning MT15040CV) except for 293T cells and cell lines derived from *RPR2;R26*^{Luc} and *RPR2;R26*^{Dll3}, which were cultured in DMEM (Hyclone SH30243.01). RPMI and DMEM were supplemented with 10% bovine growth serum (Hyclone SH3054103HI) and penicillin-streptomycin-glutamine (Gibco 10378016). Cells were grown at 37ºC in standard cell culture incubators. All cells were routinely tested (MycoAlert Detection Kit, Lonza) and confirmed to be free of mycoplasma contamination.

NCI-H524, NCI-H82, and NCI-H1694 cells were purchased from ATCC. Murine KP11B6 (a negative control for tdTomato expression) and HES1$^{GFP/+}$ SCLC cell lines were generated in the lab and have been described (Lim et al., 2017).

Lentiviral transduction

$5x10^5$ 293T cells were seeded in each well of 6-well plate and left to adhere overnight in antibiotics free DMEM supplemented with 10% bovine growth serum. Lentiviral vectors were co-transfected with delta8.2 and VSV-G lentiviral packaging vectors using PEI. The supernatant was collected after 48 hr and added to the target cells. Cells were treated on day 5 with the selection agent according to the lentiviral vector used.

Plasmids/sequences

For mammalian expression of DLL3, mouse DLL3 with a C-terminal FLAG-tag was cloned into the pCDH lentiviral expression vector.

Flow cytometry

Flow cytometry was performed using a 100 µm nozzle on BD FACSAria II (Stanford Stem Cell Institute FACS Core) and analyzed with the FACSDiva software. For single cell analysis of lung tumors sequential gating strategy was used to analyze cancer cells by staining with the following FACS antibodies (**Figure S3F**): CD45-Pacific Blue (BioLegend 103126, 1:100), CD31-Pacific Blue (BioLegend 102422, 1:100), TER-119-Pacific Blue (BioLegend 116232, 1:100), CD24-APC (eBioscience 17-0242-82, 1:200), ICAM1-PE-CY7 (BioLegend 116122, 1:100), and NCAM-PE (R&D Systems FAB7820P, 1:100) (Shue et al., 2022). Data were analyzed using Flowjo software.

Lateral inhibition with mutual inactivation (LIMI) model with DLL3

Notch receptor (N_i) in cell *i* interact with DLL1 (D_j) on the surface of a neighboring cell *j*. This *trans*-activation leads to cleavage of the Notch receptor, which frees the intracellular domain, NICD (S_i) to induce expression of the downstream genes such as Hes1 (H_i), described by the class lateral inhibition model (Collier et al., 1996). Notch receptor (N_i) also interact with DLL1 (D_i) on the same cell surface, which leads to cis-inhibition, described by the LIMI model (Sprinzak et al., 2010). In order to see the effect of cis-inhibition by DLL3 ($D3_i$), Notch receptor (N_i) and DLL1 (D_i) on the same cell surface, we modified LIMI by considering the following system in two-dimensional array:

$N_i + D_j \rightleftharpoons [N_iD_j] \rightarrow S_i$	trans-activation
$S_i \rightarrow H_i$	Induction of Hes1 expression by Notch cleavage
$H_i \dashv D_i$	Repression of DLL1
$N_i + D_i \rightleftharpoons [N_iD_i] \rightarrow \emptyset$	cis-inhibition between Notch and DLL1
$N_i + D3_i \rightleftharpoons [N_iD3_i] \rightarrow \emptyset$	cis-inhibition between DLL3 and Notch

The first four reactions that do not describe DLL3 are directly from LIMI (Sprinzak et al., 2010). This model can be described by the following set of equations applied to a two-dimensional hexagonal lattice of cells:

$$\dot{N}_i = \beta_N - \gamma_N N_i - \frac{N_i D_j}{k_t} - \frac{N_i D_i}{k_c} - \frac{N_i D3_i}{k_e} \quad (1)$$

$$\dot{D}_i = \beta_D \frac{k_{DH}}{k_{DH} + {H_i}^m} - \gamma_D D_i - \frac{N_j D_i}{k_t} - \frac{N_i D_i}{k_c} \quad (2)$$

$$\dot{H}_i = \beta_H \frac{\left(\frac{N_i D_j}{k_t \gamma_s}\right)^p}{k_{HS} + \left(\frac{N_i D_j}{k_t \gamma_s}\right)^p} - \gamma_H H_i \quad (3)$$

$$\dot{D3}_i = \beta_{D3} - \gamma_{D3} D3_i - \frac{N_i D3_i}{k_e} \quad (4)$$

Equations 1-3 are from LIMI (Sprinzak et al., 2011). N_i and D_j interact at a rate k_t^{-1}. N_i and D_i interact at a rate k_c^{-1}. N_i, D_i, and H_i are produced at a rate of β_N, β_D, and β_H, respectively. N_i, D_i, and H_i are degraded at a rate of γ_N, γ_D, and γ_H, respectively. Repression of D_i by H_i is represented with a decreasing Hill function as a function of k_{DH} and m. Expression of H_i by S_i is represented with an increasing Hill function as a function of k_{HS} and p. Equation 4 describes $D3_i$, where $D3_i$ is produced, degraded, and interact with N_i at a rate β_{D3}, γ_{D3}, and k_e, respectively. These equations are used in Figure 1.

Numerical computations were performed using MATLAB's ode15s solver (R2017b, MathWorks) using the scripts provided by Formosa-Jordan and Sprinzak (Formosa-Jordan and Sprinzak, 2014).

Mouse models

The *Rb1*$^{flox/flox}$*;Trp53*$^{flox/flox}$*;Rbl2*$^{flox/flox}$ *(RPR2,* or *TKO)* mouse model and the *Rosa26*$^{lox\text{-}stop\text{-}lox\text{-}luciferase}$ *(R26*^{Luc}*)* allele have been previously described (Jahchan et al., 2016; Schaffer et al., 2010). Mice were maintained in a mixed C57BL/6;129SVJ background.

Cre-inducible DLL3-overexpressing mice (*R26*$^{LSL\text{-}Dll3}$) were generated by knocking in a *Lox-Stop-Lox-Dll3-IRES-tdTomato* cassette into the *Rosa26* allele. The mice were generated by genOway via homologous recombination into the *Rosa26* allele in mouse embryonic stem cells, and clones were then injected into blastocysts to generate chimeric mice with for germline transmission. The *Dll3* sequence in this allele is a cDNA/gDNA combo that retains intron 6 within the cDNA sequence to allow for expression of potential splice variants.

R26$^{LSL\text{-}Dll3}$ mice were crossed to *RPR2;R26*$^{LSL\text{-}Luc}$ mice to generate *RPR2;R26*$^{LSL\text{-}Dll3/LSL\text{-}Luc}$ mice, which were then crossed to each other to generate *RPR2;R26*$^{LSL\text{-}Dll3/LSL\text{-}Dll3}$ mice and *RPR2;R26*$^{LSL\text{-}Luc/LSL\text{-}Luc}$ littermate controls. Tumors were initiated at 8-

12 weeks of age with intratracheal instillation of $4x10^7$ plaque-forming units of Adeno-CMV-Cre (Baylor College of Medicine, Houston, TX). Animals were euthanized and tumors were collected at ~6.5 months post-initiation, or earlier if they showed signs of respiratory distress. Mice were housed at 22°C ambient temperature with 40% humidity and a light/dark cycle of 12 h (7am – 7pm).

Genotyping

Mice were genotyped by using the Mouse Direct PCR kit (Bimake) on DNA isolated from tails following the manufacturer's protocol.

	Forward	Reverse
Rb1^{flox}	5'-CCTTGACCATAGCCCAGCAC-3'	5'-CTCTAGATCCTCTCATTCTTCCC-3'
p53^{flox}	5'-GAAGACAGAAAAGGGGAGGG-3'	5'-AAGGGGTATGAGGGACAAGG-3'
Rbl2^{flox}	5'-GACTGCTGGTATTAGAACCC-3'	5'-GTGTTGTAACATTCTCGTGGG-3'
R26^{Luc}	5'-AAAGTCGCTCTGAGTTGTTAT-3'	5'-GCGAAGAGTTTGTCCTCAACC-3'
R26$^{LSL\text{-}Dll3}$	5'-AAGAAAAGCCAGGATCAGCGTCTGG-3'	5'-CACTGCATTCTAGTTGTGGTTTGTCCAAAC-3'
R26^{Dll3}	5'-AAGAAAAGCCAGGATCAGCGTCTGG-3'	5'-GGGCAACGTGCTGGTTATTG-3'
tdTomato	5'-TGGAGTGGCAACTTCCAGGG-3'	5'-ACGGCATGGACGAGCTGTA-3'

Immunostaining

Lung lobes were fixed overnight in 10% formalin in PBS before paraffin embedding. Paraffin sections were deparaffinized with Histo-Clear (National Diagnostics HS-200) and gradually rehydrated from ethanol to water. Antigen retrieval was carried out in citrate-based unmasking solution (Vector Laboratories H-3300) by microwaving at full power until boiling, then 30% power for 25 min (DLL3) or 15 min (HES1), then left to cool at room temperature for 10 min before washing with water. Endogenous peroxidase was blocked by incubating slides in 3% hydrogen peroxide for 1 h. Sections were washed in PBST (PBS with 0.1% Tween-20), blocked in 5% horse serum for 1 h, and incubated with anti-DLL3 (1:200 Invitrogen PA5-23448) or anti-HES1 (1:200 Cell Signaling Technology 11988) diluted in PBST overnight at 4°C. DLL3 was developed using ImmPRESS®HRP Horse Anti-Rabbit IgG Polymer Detection Kit (Vector Laboratories MP-7401) following the manufacturer's protocol. HES1 was developed using ImmPRESS® Excel Amplified

Polymer Staining Anti-Rabbit IgG Peroxidase Kit (Vector Laboratories MP-7601) following the manufacturer's protocol. All sections used DAB substrate kit (Vector Laboratories SK-4100) for color development. Sections were counterstained with hematoxylin (Sigma-Aldrich HHS32-1L), gradually dehydrated from water to ethanol to xylene, and mounted with Refrax mounting medium (Anatech Ltd711). Sections were imaged using Keyence BZ-X700 all-in-one fluorescence microscope with BZ-X Viewer program version 1.3.1.1 and BZ-X Analyzer 1.4.0.1.

Single-cell suspension

Tumors were dissected from lungs between 5 to 6.5 months after tumor induction, finely chopped with a razor blade, and digested for 15 min at 37°C in 10 mL of L-15 medium (Sigma L1518) containing 4.25 mg/mL Collagenase I (Sigma C0130), 1.4 mg/mL Collagenase II (Sigma 6885), 4.25 mg/mL Collagenase IV (Sigma 5138), 0.625 mg/mL Elastase (Worthington LS002292), and 0.625 mg/mL DNase I (Roche 10104159). The digested mixture was filtered through a 40 µm filter and centrifuged at 400 g for 5 min at room temp, and the resulting pellet was resuspended in 1 mL RBC lysis buffer (eBioscience 00-4333-57) for 30 sec, diluted in 30 mL PBS, and centrifuged at 400 g for 5 min at room temp. The pelleted cells were then resuspended in 0.1% BSA/PBS for flow cytometry or in cell culture media to generate cell lines.

Statistical analysis

Statistical significance was assayed with GraphPad Prism software. Data are represented as mean ± sd. *$p<0.05$, **$p<0.01$, ***$p<0.001$, ****$p<0.0001$, ns not significant. The tests used are indicated in the figure legend.

Data availability

All data are available in the article or from the corresponding author upon request.

Acknowledgements

The authors thank Dr. Laura Saunders and Dr. Chen-Hua Chuang at Abbvie/StemCentrx for their help during the course of this study, including with the generation of the *R26*$^{LSL\text{-}Dll3}$ mice. We would like to thank David S. Glass for discussions and advice. We also thank Pauline Chu from the Stanford Histology Service Center and all the members of the Sage lab for their help throughout this study. Research reported in this publication was supported by the Ludwig Institute for Cancer Research (J.S.), the NIH (grants CA217450, CA213273, and CA231997 to J.S., CA257169 to J.H.K.), and the A.P. Giannini Foundation (J.W.K.).

Contributions

J.W.K., J.H.K, and J.S. designed the experiments, interpreted the results, and wrote the manuscript; J.W.K. performed the mathematical modeling and developed the scFv molecules; J.H.K performed experiments with mice; J.W.K. and J.H.K. worked together on experiments with cells in culture and tumor analysis.

Competing interests

J.S. received research funding from StemCentrx/Abbvie for the development of the new *Dll3* allele. J.S. has equity in, and is an advisor for, DISCO Pharmaceuticals. The authors declare no other competing interests.

References

Baine, M.K., Hsieh, M.-S.S., Lai, W.V., Egger, J.V., Jungbluth, A.A., Daneshbod, Y., Beras, A., Spencer, R., Lopardo, J., Bodd, F., Montecalvo, J., Sauter, J.L., Chang, J.C., Buonocore, D.J., Travis, W.D., Sen, T., Poirier, J.T., Rudin, C.M., Rekhtman, N., Victoria Lai, W., Egger, J.V., Jungbluth, A.A., Daneshbod, Y., Beras, A., Spencer, R., Lopardo, J., Bodd, F., Montecalvo, J., Sauter, J.L., Chang, J.C., Buonocore, D.J., Travis, W.D., Sen, T., Poirier, J.T., Rudin, C.M., Rekhtman, N., Lai, W.V., Egger, J.V., Jungbluth, A.A., Daneshbod, Y., Beras, A., Spencer, R., Lopardo, J., Bodd, F., Montecalvo, J., Sauter, J.L., Chang, J.C., Buonocore, D.J., Travis, W.D., Sen, T., Poirier, J.T., Rudin, C.M., Rekhtman, N., 2020. SCLC Subtypes Defined by ASCL1, NEUROD1, POU2F3, and YAP1: A Comprehensive Immunohistochemical and Histopathologic Characterization. Journal of Thoracic Oncology 15, 1823–1835. https://doi.org/10.1016/j.jtho.2020.09.009

Barrows, E.D., Blackburn, M.J., Liu, S.V., 2022. Evolving role of immunotherapy in small cell lung cancer. Semin Cancer Biol S1044-579X(22)00048–7. https://doi.org/10.1016/j.semcancer.2022.02.021

Black, J.R.M., McGranahan, N., 2021. Genetic and non-genetic clonal diversity in cancer evolution. Nat Rev Cancer 21, 379–392. https://doi.org/10.1038/s41568-021-00336-2

Blackhall, F., Jao, K., Greillier, L., Cho, B.C., Penkov, K., Reguart, N., Majem, M., Nackaerts, K., Syrigos, K., Hansen, K., Schuette, W., Cetnar, J., Cappuzzo, F., Okamoto, I., Erman, M., Langer, S.W., Kato, T., Groen, H., Sun, Z., Luo, Y., Tanwani, P., Caffrey, L., Komarnitsky, P., Reinmuth, N., 2021. Efficacy and Safety of Rovalpituzumab Tesirine Compared With Topotecan as Second-Line Therapy in DLL3-High SCLC: Results From the Phase 3 TAHOE Study. Journal of Thoracic Oncology 16, 1547–1558. https://doi.org/10.1016/j.jtho.2021.02.009

Bocci, F., Gearhart-Serna, L., Boareto, M., Ribeiro, M., Ben-Jacob, E., Devi, G.R., Levine, H., Onuchic, J.N., Jolly, M.K., 2019. Toward understanding cancer stem cell heterogeneity in the tumor microenvironment. Proc Natl Acad Sci U S A 116, 148–157. https://doi.org/10.1073/pnas.1815345116

Bulman, M.P., Kusumi, K., Frayling, T.M., McKeown, C., Garrett, C., Lander, E.S., Krumlauf, R., Hattersley, A.T., Ellard, S., Turnpenny, P.D., 2000. Mutations in the human delta homologue, DLL3, cause axial skeletal defects in spondylocostal dysostosis. Nat Genet 24, 438–441. https://doi.org/10.1038/74307

Calbo, J., van Montfort, E., Proost, N., van Drunen, E., Beverloo, H.B., Meuwissen, R., Berns, A., 2011. A functional role for tumor cell heterogeneity in a mouse model of small cell lung cancer. Cancer Cell 19, 244–256. https://doi.org/10.1016/j.ccr.2010.12.021

Chapman, G., Sparrow, D.B., Kremmer, E., Dunwoodie, S.L., 2011. Notch inhibition by the ligand DELTA-LIKE 3 defines the mechanism of abnormal vertebral segmentation in spondylocostal dysostosis. Hum Mol Genet 20, 905–916. https://doi.org/10.1093/hmg/ddq529

Chitnis, A.B., 1995. The role of Notch in lateral inhibition and cell fate specification. Mol Cell Neurosci 6, 311–321.

Collier, J.R., Monk, N.A., Maini, P.K., Lewis, J.H., 1996. Pattern formation by lateral inhibition with feedback: a mathematical model of delta-notch intercellular signalling. J Theor Biol 183, 429–446. https://doi.org/10.1006/jtbi.1996.0233

Dagogo-Jack, I., Shaw, A.T., 2018. Tumour heterogeneity and resistance to cancer therapies. Nat Rev Clin Oncol 15, 81–94. https://doi.org/10.1038/nrclinonc.2017.166

Dunwoodie, S.L., Henrique, D., Harrison, S.M., Beddington, R.S., 1997. Mouse Dll3: a novel divergent Delta gene which may complement the function of other Delta homologues during early pattern formation in the mouse embryo. Development 124, 3065–3076. https://doi.org/10.1242/dev.124.16.3065

Formosa-Jordan, P., and D. Sprinzak. 2014. 'Modeling Notch signaling: a practical tutorial', *Methods Mol Biol*, 1187: 285-310.

Gay, C.M., Stewart, C.A., Park, E.M., Diao, L., Groves, S.M., Heeke, S., Nabet, B.Y., Fujimoto, J., Solis, L.M., Lu, W., Xi, Y., Cardnell, R.J., Wang, Q., Fabbri, G., Cargill, K.R., Vokes, N.I., Ramkumar, K., Zhang, B., Della Corte, C.M., Robson, P., Swisher, S.G., Roth, J.A., Glisson, B.S., Shames, D.S., Wistuba, I.I., Wang, J., Quaranta, V., Minna, J., Heymach, J.V., Byers, L.A., 2021. Patterns of transcription factor programs and immune pathway activation define four major subtypes of SCLC with distinct therapeutic vulnerabilities. Cancer Cell 39, 346-360.e7. https://doi.org/10.1016/j.ccell.2020.12.014

Geffers, I., Serth, K., Chapman, G., Jaekel, R., Schuster-Gossler, K., Cordes, R., Sparrow, D.B., Kremmer, E., Dunwoodie, S.L., Klein, T., Gossler, A., 2007. Divergent functions and distinct localization of the Notch ligands DLL1 and DLL3 in vivo. The Journal of Cell Biology 178, 465. https://doi.org/10.1083/JCB.200702009

Giffin, M.J., Cooke, K., Lobenhofer, E.K., Estrada, J., Zhan, J., Deegen, P., Thomas, M., Murawsky, C.M., Werner, J., Liu, S., Lee, F., Homann, O., Friedrich, M., Pearson, J.T., Raum, T., Yang, Y., Caenepeel, S., Stevens, J., Beltran, P.J., Canon, J., Coxon, A., Bailis, J.M., Hughes, P.E., 2021. AMG 757, a half-life extended, DLL3-targeted bispecific T-cell engager, shows high potency and sensitivity in preclinical models of small-cell lung cancer. Clinical Cancer Research 27, 1526–1537. https://doi.org/10.1158/1078-0432.CCR-20-2845

Hipp, S., Voynov, V., Drobits-Handl, B., Giragossian, C., Trapani, F., Nixon, A.E., Scheer, J.M., Adam, P.J., 2020. A Bispecific DLL3/CD3 IgG-Like T-Cell Engaging Antibody Induces Antitumor Responses in Small Cell Lung Cancer. Clin Cancer Res 26, 5258–5268. https://doi.org/10.1158/1078-0432.CCR-20-0926

Ireland, A.S., Micinski, A.M., Kastner, D.W., Guo, B., Wait, S.J., Spainhower, K.B., Conley, C.C., Chen, O.S., Guthrie, M.R., Soltero, D., Qiao, Y., Huang, X., Tarapcsák, S., Devarakonda, S., Chalishazar, M.D., Gertz, J., Moser, J.C., Marth, G., Puri, S., Witt, B.L., Spike, B.T., Oliver, T.G., 2020. MYC Drives Temporal Evolution of Small Cell Lung Cancer Subtypes by Reprogramming Neuroendocrine Fate. Cancer cell. https://doi.org/10.1016/j.ccell.2020.05.001

Jahchan, N.S., Lim, J.S., Bola, B., Peifer, M., 2016. Identification and Targeting of Long-Term Tumor- Propagating Cells in Small Cell Lung Cancer. https://doi.org/10.1016/j.celrep.2016.06.021

Jamal-Hanjani, M., Quezada, S.A., Larkin, J., Swanton, C., 2015. Translational implications of tumor heterogeneity. Clin Cancer Res 21, 1258–1266. https://doi.org/10.1158/1078-0432.CCR-14-1429

Johnson, M.L., Zvirbule, Z., Laktionov, K., Helland, A., Cho, B.C., Gutierrez, V., Colinet, B., Lena, H., Wolf, M., Gottfried, M., Okamoto, I., van der Leest, C., Rich, P., Hung, J.-Y., Appenzeller, C., Sun, Z., Maag, D., Luo, Y., Nickner, C., Vajikova, A., Komarnitsky, P., Bar, J., 2021. Rovalpituzumab Tesirine as a Maintenance Therapy After First-Line Platinum-Based Chemotherapy in Patients With Extensive-Stage-SCLC: Results From the Phase 3 MERU Study. J Thorac Oncol 16, 1570–1581. https://doi.org/10.1016/j.jtho.2021.03.012

Kusumi, K., Sun, E.S., Kerrebrock, A.W., Bronson, R.T., Chi, D.C., Bulotsky, M.S., Spencer, J.B., Birren, B.W., Frankel, W.N., Lander, E.S., 1998. The mouse pudgy mutation disrupts Delta homologue Dll3 and initiation of early somite boundaries. Nature genetics 19, 274–278. https://doi.org/10.1038/961

Ladi, E., Nichols, J.T., Ge, W., Miyamoto, A., Yao, C., Yang, L.T., Boulter, J., Sun, Y.E., Kintner, C., Weinmaster, G., 2005. The divergent DSL ligand Dll3 does not activate Notch signaling but cell autonomously attenuates signaling induced by other DSL ligands. Journal of Cell Biology 170, 983–992. https://doi.org/10.1083/jcb.200503113

Lakes, A.L., An, D.D., Gauny, S.S., Ansoborlo, C., Liang, B.H., Rees, J.A., McKnight, K.D., Karsunky, H., Abergel, R.J., 2020. Evaluating 225Ac and 177Lu Radioimmunoconjugates against Antibody-Drug Conjugates for Small-Cell Lung Cancer. Mol Pharm 17, 4270–4279. https://doi.org/10.1021/acs.molpharmaceut.0c00703

Lim, J.S., Ibaseta, A., Fischer, M.M., Cancilla, B., O'Young, G., Cristea, S., Luca, V.C., Yang, D., Jahchan, N.S., Hamard, C., Antoine, M., Wislez, M., Kong, C., Cain, J., Liu, Y.-W., Kapoun, A.M., Garcia, K.C., Hoey, T., Murriel, C.L., Sage, J., 2017. Intratumoural heterogeneity generated by Notch signalling promotes small-cell lung cancer. Nature 545, 360–364. https://doi.org/10.1038/nature22323

Lim, K.J., Brandt, W.D., Heth, J.A., Muraszko, K.M., Fan, X., Bar, E.E., Eberhart, C.G., 2015. Lateral inhibition of Notch signaling in neoplastic cells. Oncotarget 6, 1666–1677. https://doi.org/10.18632/oncotarget.2762

Malhotra, J., Nikolinakos, P., Leal, T., Lehman, J., Morgensztern, D., Patel, J.D., Wrangle, J.M., Curigliano, G., Greillier, L., Johnson, M.L., Ready, N., Robinet, G., Lally, S., Maag, D., Valenzuela, R., Blot, V., Besse, B., 2021. A Phase 1-2 Study of Rovalpituzumab Tesirine in Combination With Nivolumab Plus or Minus Ipilimumab in Patients With Previously Treated Extensive-Stage SCLC. J Thorac Oncol 16, 1559–1569. https://doi.org/10.1016/j.jtho.2021.02.022

Nelson, B.R., Hartman, B.H., Ray, C.A., Hayashi, T., Bermingham-McDonogh, O., Reh, T.A., 2009. Acheate-scute like 1 (Ascl1) is required for normal delta-like (Dll) gene expression and notch signaling during retinal development. Dev Dyn 238, 2163–2178. https://doi.org/10.1002/dvdy.21848

Ohsawa, R., Kageyama, R., 2008. Regulation of retinal cell fate specification by multiple transcription factors. Brain Res 1192, 90–98. https://doi.org/10.1016/j.brainres.2007.04.014

Peltomaa, R., Barderas, R., Benito-Peña, E., Moreno-Bondi, M.C., 2022. Recombinant antibodies and their use for food immunoanalysis. Anal Bioanal Chem 414, 193–217. https://doi.org/10.1007/s00216-021-03619-7

Raum, T., Blümel, C., Dahlhoff, C., Hoffmann, P., Kufer, P., Lutterbüse, R., Nahrwold, E., Pendzialek, J., 2017. Antibody constructs for dll3 and cd3. US20170037130A1.

Rudin, C.M., Brambilla, E., Faivre-Finn, C., Sage, J., 2021. Small-cell lung cancer. Nature Reviews Disease Primers 7, 1–20. https://doi.org/10.1038/s41572-020-00235-0

Rudin, C.M., Poirier, J.T., Byers, L.A., Dive, C., Dowlati, A., George, J., Heymach, J.V., Johnson, J.E., Lehman, J.M., MacPherson, D., Massion, P.P., Minna, J.D., Oliver, T.G., Quaranta, V., Sage, J., Thomas, R.K., Vakoc, C.R., Gazdar, A.F., 2019. Molecular subtypes of small cell lung cancer: a synthesis of human and mouse model data. Nat Rev Cancer 19, 289–297. https://doi.org/10.1038/s41568-019-0133-9

Saunders, L.R., Bankovich, A.J., Anderson, W.C., Aujay, M.A., Bheddah, S., Black, K.A., Desai, R., Escarpe, P.A., Hampl, J., Laysang, A., Liu, D., Lopez-Molina, J., Milton, M., Park, A., Pysz, M.A., Shao, H., Slingerland, B., Torgov, M., Williams, S.A., Foord, O., Howard, P., Jassem, J., Badzio, A., Czapiewski, P., Harpole, D.H., Dowlati, A., Massion, P.P., Travis, W.D., Pietanza, M.C., Poirier, J.T., Rudin, C.M., Stull, R.A., Dylla, S.J., 2015. A DLL3-targeted antibody-drug conjugate eradicates high-grade pulmonary neuroendocrine tumor-initiating cells in vivo. Science Translational Medicine 7. https://doi.org/10.1126/scitranslmed.aac9459

Schaffer, B.E., Park, K.S., Yiu, G., Conklin, J.F., Lin, C., Burkhart, D.L., Karnezis, A.N., Sweet-Cordero, E.A., Sage, J., 2010. Loss of p130 accelerates tumor development in a mouse model for human small-cell lung carcinoma. Cancer Research 70, 3877–3883. https://doi.org/10.1158/0008-5472.CAN-09-4228

Serth, K., Schuster-Gossler, K., Kremmer, E., Hansen, B., Marohn-Köhn, B., Gossler, A., 2015. O-fucosylation of DLL3 is required for its function during somitogenesis. PLoS One 10, e0123776. https://doi.org/10.1371/journal.pone.0123776

Sharma, S.K., Pourat, J., Abdel-Atti, D., Carlin, S.D., Piersigilli, A., Bankovich, A.J., Gardner, E.E., Hamdy, O., Isse, K., Bheddah, S., Sandoval, J., Cunanan, K.M., Johansen, E.B., Allaj, V., Sisodiya, V., Liu, D., Zeglis, B.M., Rudin, C.M., Dylla, S.J., Poirier, J.T., Lewis, J.S., 2017. Noninvasive interrogation of DLL3 expression in metastatic small cell lung cancer. Cancer Research 77, 3931–3941. https://doi.org/10.1158/0008-5472.CAN-17-0299

Shue, Y.T., Drainas, A.P., Li, N.Y., Pearsall, S.M., Morgan, D., Sinnott-Armstrong, N., Hipkins, S.Q., Coles, G.L., Lim, J.S., Oro, A.E., Simpson, K.L., Dive, C., Sage, J., 2022. A conserved YAP/Notch/REST network controls the neuroendocrine cell fate in the lungs. Nat Commun 13, 1–18. https://doi.org/10.1038/s41467-022-30416-2

Sjöqvist, M., Andersson, E.R., 2019. Do as I say, Not(ch) as I do: Lateral control of cell fate. Dev Biol 447, 58–70. https://doi.org/10.1016/j.ydbio.2017.09.032

Stewart, C.A., Gay, C.M., Xi, Y., Sivajothi, S., Sivakamasundari, V., Fujimoto, J., Bolisetty, M., Hartsfield, P.M., Balasubramaniyan, V., Chalishazar, M.D., Moran, C., Kalhor, N., Stewart, J., Tran, H., Swisher, S.G., Roth, J.A., Zhang, J., de Groot, J., Glisson, B., Oliver, T.G., Heymach, J.V., Wistuba, I., Robson, P., Wang, J., Byers, L.A.,

2020. Single-cell analyses reveal increased intratumoral heterogeneity after the onset of therapy resistance in small-cell lung cancer. Nat Cancer 1, 423–436. https://doi.org/10.1038/s43018-019-0020-z

Sutherland, K.D., Ireland, A.S., Oliver, T.G., 2022. Killing SCLC: insights into how to target a shapeshifting tumor. Genes Dev 36, 241–258. https://doi.org/10.1101/gad.349359.122

Tammela, T., Sage, J., 2020. Investigating Tumor Heterogeneity in Mouse Models. Annu Rev Cancer Biol 4, 99–119. https://doi.org/10.1146/annurev-cancerbio-030419-033413

Torab, P., Yan, Y., Ahmed, M., Yamashita, H., Warrick, J.I., Raman, J.D., DeGraff, D.J., Wong, P.K., 2021. Intratumoral Heterogeneity Promotes Collective Cancer Invasion through NOTCH1 Variation. Cells 10, 3084. https://doi.org/10.3390/cells10113084

Tully, K.M., Tendler, S., Carter, L.M., Sharma, S.K., Samuels, Z.V., Mandleywala, K., Korsen, J.A., Delos Reyes, A.M., Piersigilli, A., Travis, W.D., Sen, T., Pillarsetty, N., Poirier, J.T., Rudin, C.M., Lewis, J.S., 2022. Radioimmunotherapy Targeting Delta-like Ligand 3 in Small Cell Lung Cancer Exhibits Antitumor Efficacy with Low Toxicity. Clinical Cancer Research 28, 1391–1401. https://doi.org/10.1158/1078-0432.ccr-21-1533

Wei, W., Rosenkrans, Z.T., Liu, J., Huang, G., Luo, Q.-Y., Cai, W., 2020. ImmunoPET: Concept, Design, and Applications. Chem Rev 120, 3787–3851. https://doi.org/10.1021/acs.chemrev.9b00738

Weisser, N.E., Hall, J.C., 2009. Applications of single-chain variable fragment antibodies in therapeutics and diagnostics. Biotechnol Adv 27, 502–520. https://doi.org/10.1016/j.biotechadv.2009.04.004

Williamson, S.C., Metcalf, R.L., Trapani, F., Mohan, S., Antonello, J., Abbott, B., Leong, H.S., Chester, C.P.E., Simms, N., Polanski, R., Nonaka, D., Priest, L., Fusi, A., Carlsson, F., Carlsson, A., Hendrix, M.J.C., Seftor, R.E.B., Seftor, E.A., Rothwell, D.G., Hughes, A., Hicks, J., Miller, C., Kuhn, P., Brady, G., Simpson, K.L., Blackhall, F.H., Dive, C., 2016. Vasculogenic mimicry in small cell lung cancer. Nature Communications 7, 1–14. https://doi.org/10.1038/ncomms13322

Figures and Figure Legends

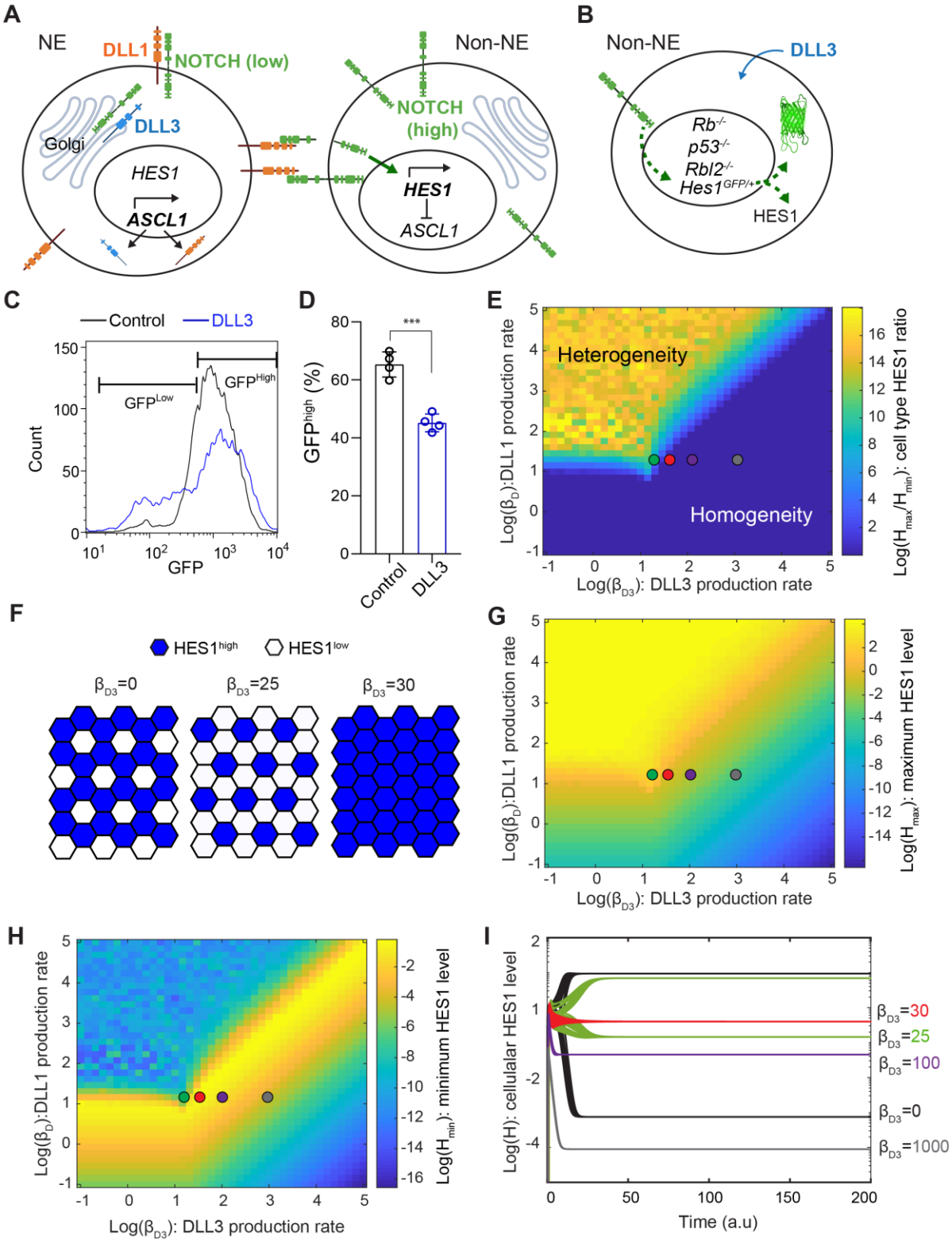

Figure 1. Mathematical model of mutual inactivation shows production rate dependent role of DLL3. (**A**) Schematic of Notch, DLL1, and DLL3 interaction in lateral

inhibition with mutual inactivation (LIMI). (**B**) Schematic of HES1^{GFP}-positive cells from an *Rb;p53;Rbl2;Hes1^{GFP}* tumor serving as a reporter cell line, with GFP expression from the *Hes1* locus to monitor the effect of DLL3 expression in regulating Notch activity. (**C**) Flow cytometry of HES1^{GFP}-positive cells with (blue) and without (black) ectopic expression of DLL3 (representative of n = 4 biological replicates). (**D**) Percentage of GFP^{high} HES1^{GFP}-positive cells with and without ectopic expression of DLL3. Unpaired t-test, data represented as mean ± s.d. ***p<0.001 (**E**) Log(H_{max}/H_{min}) at steady state were calculated as a function of β_{DLL3} and β_D. Regions with values greater than 0 (light blue to yellow regions) support patterning, while those with 0 (dark blue) do not. (**F**) Hexagonal cell lattice with LIMI showing that DLL3 expression can lead to sparser patterns of higher HES1 cells (blue) or no pattern (homogeneous color). (**G**) H_{max} as a function of β_{DLL3} and β_D. (**H**) H_{min} as a function of β_{DLL3} and β_D. (**I**) Simulations with the indicated parameters for β_{DLL3} showing H levels in cells with high and low final H levels. Green, red, purple, and gray dots in (E), (G), and (H) correspond to the parameters used in (I).

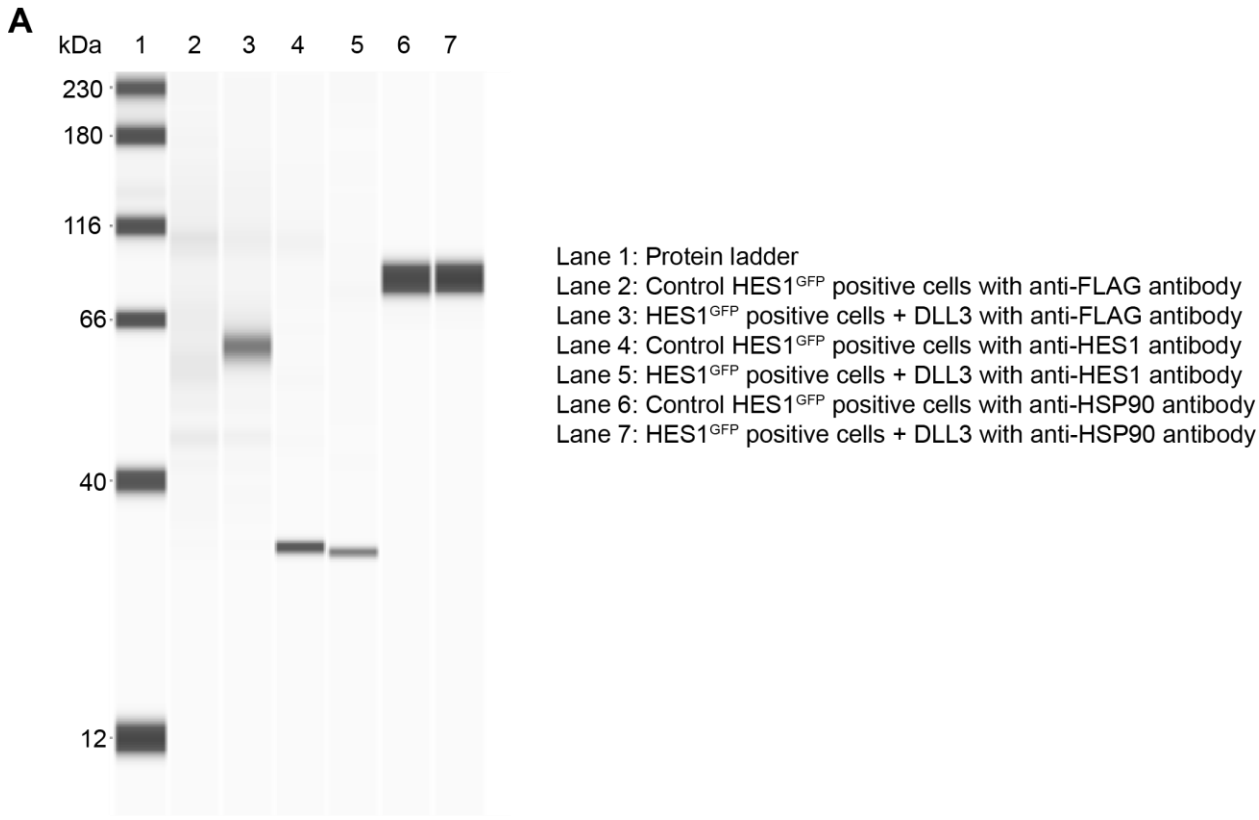

Figure S1 related to Figure 1. Ectopic expression of DLL3 in HES1^{GFP}-positive cells. (**A**) Immunoassay measuring DLL3 and HES1 expression in control HES1^{GFP}-positive cells and the same cells with stable expression of DLL3. HSP90 serves as a loading control. The expected molecular weights of DLL3, HES1, and HSP90 are 65 kDa, 30 kDa, and 90 kDa, respectively.

Table S1 related to Figure 1: Parameter values for mathematical modeling

See equations in Methods and Figure 1

Figure	Equations	Parameters	Initial conditions
1E,G,H	1–4	$\gamma = 1$, $k_e = 0.1$, $k_{DR} = 1$, $k_f = 0.1$, $Y_s = 1$, $p = 3$, $k_{RS} = 300000$, $Y_R = 1$, $\beta_N = 20$, $\beta_H = 1000000$, $m = 1$, sigma = 0.1, $k_c = 0.1$, $k_t = 1$, β_D = 1 to 1e3, β_{D3} = 1 to 1e3	Cells initially set in low values of NOTCH, DLL1, and DLL3 with small variability.
1F	1–4	$\gamma = 1$, $k_e = 0.1$, $k_{DR} = 1$, $k_f = 0.1$, $Y_s = 1$, $p = 3$, $k_{RS} = 300000$, $Y_R = 1$, $\beta_D = 15$, $\beta_N = 20$, $\beta_H = 1000000$, $m = 1$, sigma = 0.1, $k_c = 0.1$, $k_t = 1$, β_{D3} = 0, 25, 30	Cells initially set in low values of NOTCH, DLL1, and DLL3 with small variability.
1I	1–4	$\gamma = 1$, $k_e = 0.1$, $k_{DR} = 1$, $k_f = 0.1$, $Y_s = 1$, $p = 3$, $k_{RS} = 300000$, $Y_R = 1$, $\beta_D = 15$, $\beta_N = 20$, $\beta_H = 1000000$, $m = 1$, sigma = 0.1, $k_c = 0.1$, $k_t = 1$, β_{D3} = 0, 25, 30, 100, 1000	Cells initially set in low values of NOTCH, DLL1, and DLL3 with small variability.

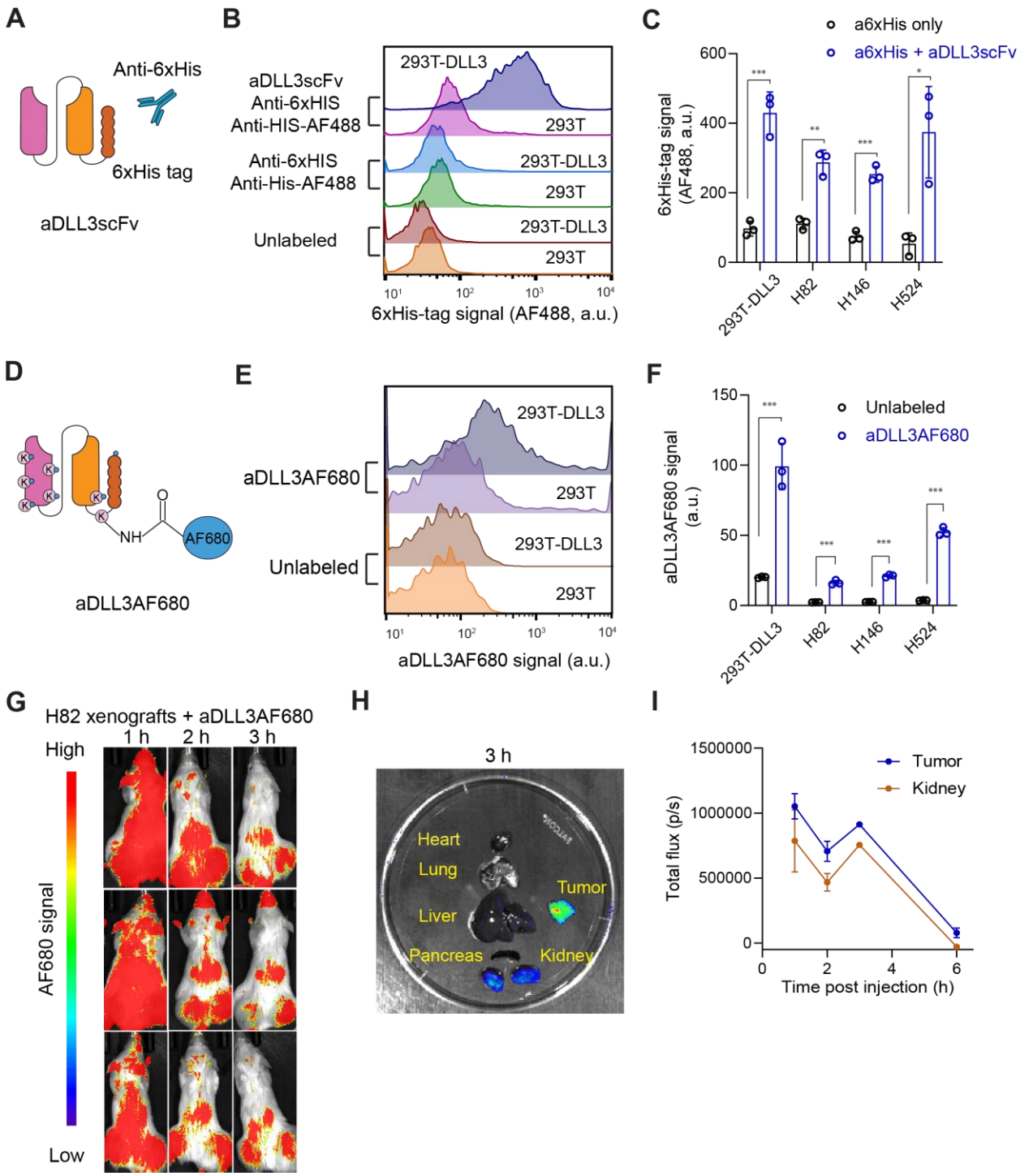

Figure 2. Detection of DLL3 expression at the surface of cells using anti-DLL3 scFv. (**A**) Schematic representation of the His-tagged scFv targeting DLL3 (aDLL3scFv) and the detection of cells expressing DLL3 using this molecule. (**B**) Representative flow cytometry analysis of DLL3 expression in 293T cells expressing exogenous mouse DLL3 using aDLL3scFv (from n=3 biological replicates). (**C**) Quantification of DLL3 detection in

human SCLC cell lines. (**D**) Schematic representation of AF680 labeled aDLL3scFv (aDLL3AF680). (**E**) Representative flow cytometry showing binding activity of aDLL3AF680 (from n=3 biological replicates). (**F**) Quantification of (E) in human SCLC cell lines. (**G**) Whole body fluorescent images of H82 tumor xenografts injected via tail vein with 2 nmol of AF680-labeled scFv. Tumors (T) and kidneys (K) are indicated. (**H**) Representative *ex vivo* imaging of an NCI-H82 bearing mice in (H). (**I**) Quantification of imaging signals, reported as the total flux (p/s) (n=3). Unpaired t-test, data represented as mean ± s.d. $p<0.05$, $^{**}p<0.01$, $^{***}p<0.001$.

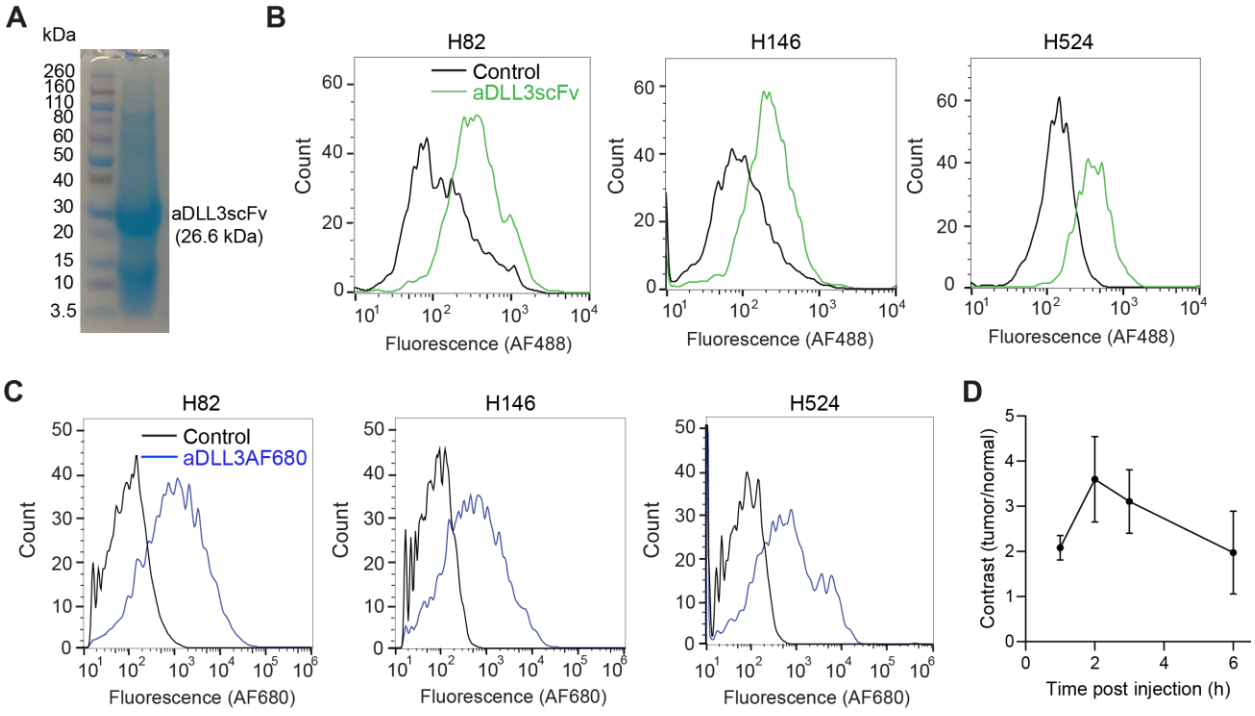

Figure S2 related to Figure 2. Anti-DLL3 scFv binds to human SCLC cells *in vitro* and *in vivo*. (**A**) SDS-PAGE gel stained with SimplyBlue Safe Stain showing aDLL3scFv purified using nickel-NTA affinity column. (**B**) Representative flow cytometry histograms showing binding of human SCLC cells to His-tagged aDLL3scFv, which was detected using rabbit anti-His antibody and AF488 labeled anti-rabbit antibody. (**C**) Representative flow cytometry histograms showing binding of aDLL3AF680 to human SCLC cells. (**D**) Quantification of imaging contrast reported as the ratio of fluorescent signals for tumor versus normal tissue. Error bars represent s.d., n = 3.

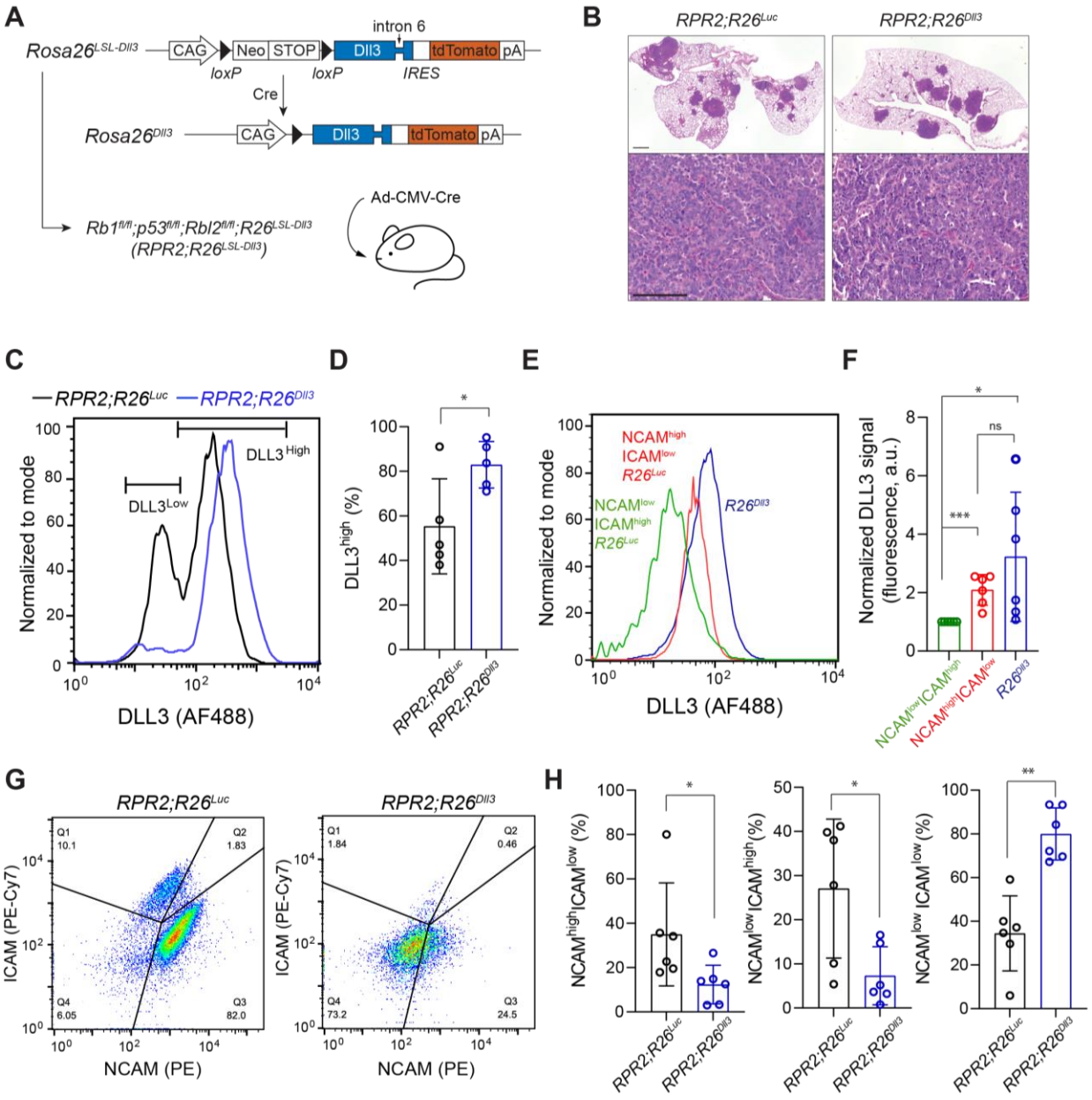

Figure 3. DLL3 expression perturbs the balance between neuroendocrine and non-neuroendocrine cells in a mouse model of SCLC. (**A**) Schematic representation of the Cre-inducible *Dll3* allele and the genetically engineered mouse model of SCLC. (**B**) Representative hematoxylin and eosin (H&E) staining of representative sections from *RPR2;R26^{luc}* and *RPR2;R26^{Dll3}* mutant lungs (top, scale bar 1mm) and lung tumors (bottom, scale bar 100μm) 6 months after tumor initiation (n ≥ 6 mice). (**C**) Representative flow cytometry analysis of DLL3 cell surface expression in SCLC cells from *RPR2;R26^{luc}*

and *RPR2;R26*^{Dll3} mutant mice 5.5 months after tumor initiation. (**D**) Quantification of (**C**) (n=5 independent experiments). (**E**) As in (C) with *RPR2;R26*^{luc} SCLC cells differentiated by NCAM and ICAM expression. (**F**) Quantification of (E) (n=6 independent experiments). (**G**) Representative flow cytometry dot plots of cells isolated from pooled tumors from *RPR2;R26*^{luc} (left) and *RPR2;R26*^{Dll3} (right). (**H**) Quantification of NCAM^{high} ICAM^{low}, NCAM^{low} ICAM^{high}, and NCAM^{low} ICAM^{low} populations in (G). Unpaired t-test, data represented as mean ± s.d. $p<0.05$, $^{**}p<0.01$, $^{***}p<0.001$.

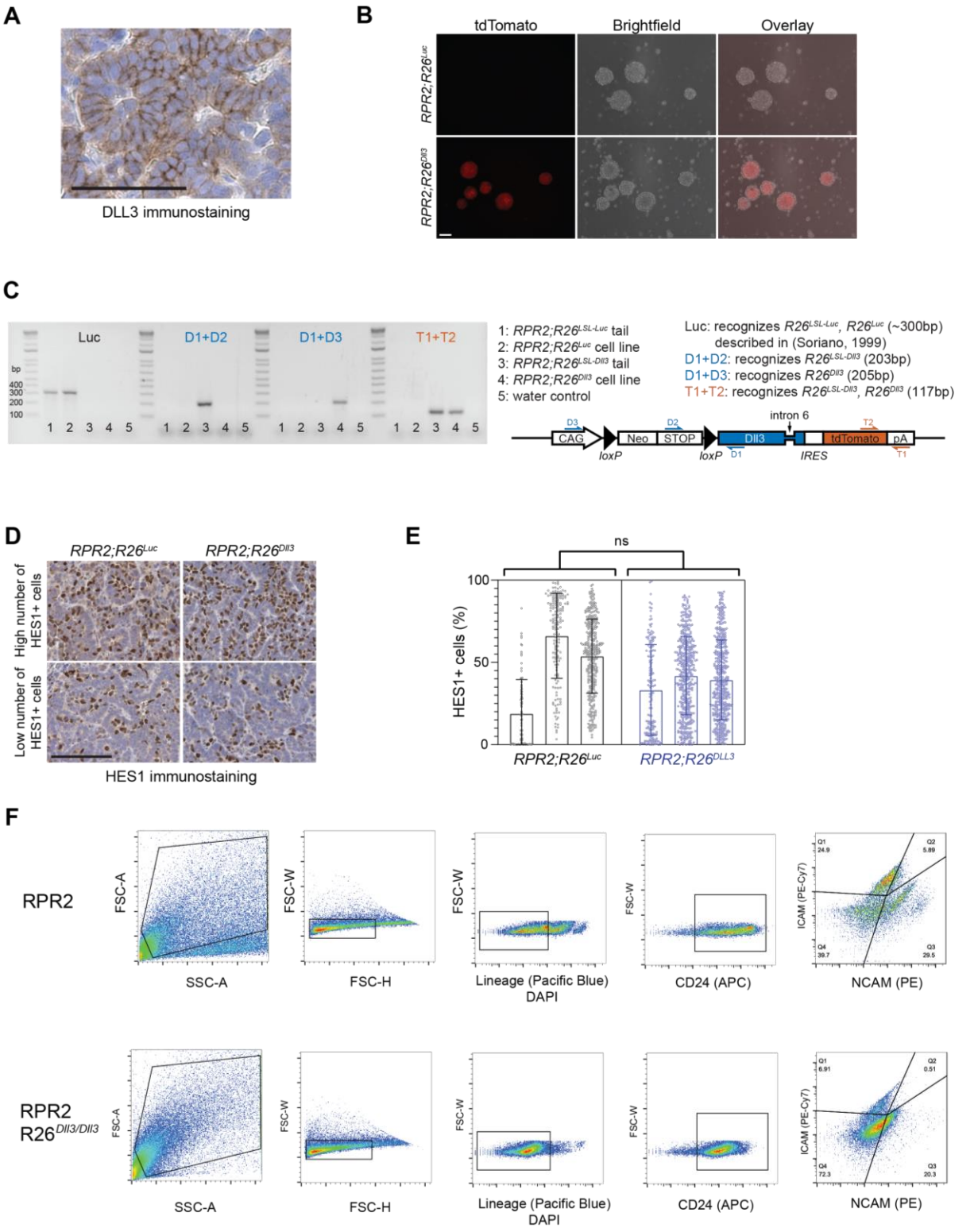

Figure S3 related to Figure 3. **Characterization of a new mouse allele with inducible expression of DLL3.** (**A**) Representative DLL3 immunostaining in an *RPR2;R26^{Luc}* mutant lung tumor section. Scale bar 50µm. (**B**) Representative tdTomato fluorescent and

brightfield images of cell lines derived from *RPR2;R26*^{Luc} (top) or *RPR2;R26*^{Dll3} (bottom) mutant lung tumors, scale bar 100µm. (**C**) Genotyping PCR and schematic of allele-specific primer pairs. DNA was extracted from the cell lines shown in (B) and from mouse tails for unrecombined controls. (**D**) Representative HES1 immunostaining in *RPR2;R26*^{Luc} (left) and *RPR2;R26*^{Dll3} (right) mutant lung tumor sections. Scale bar 100µm. (**E**) Quantification of (D). Each point is a 100 µm diameter region within a tumor, and each bar represents a section from an individual mouse. p=0.597 by nested t-test. Error bars represent SD. (**F**) Flow cytometry strategy to analyze NCAM^{high} ICAM^{low} and NCAM^{low} ICAM^{high} SCLC cells from RPR2;R26^{luc} (top) and RPR2;R26^{Dll3} (bottom) mutant mouse SCLC tumors.